Part Three
Characterization Techniques of Measuring Stresses on the Nanoscale

Mechanical Stress on the Nanoscale: Simulation, Material Systems and Characterization Techniques, First Edition.
Edited by Margrit Hanbücken, Pierre Müller, and Ralf B. Wehrspohn.
© 2011 Wiley-VCH Verlag GmbH & Co. KGaA. Published 2011 by Wiley-VCH Verlag GmbH & Co. KGaA.

9
Strain Analysis in Transmission Electron Microscopy: How Far Can We Go?

Anne Ponchet, Christophe Gatel, Christian Roucau, and Marie-José Casanove

Nanostructures are characterized by dimensions in the range of 1–100 nm in at least one direction; this definition includes 2D structures (quantum wells, thin layers), 1D structures (quantum wires, nanowires, etc.), and the so-called 0D structures (quantum dots, nanoparticles, etc.). Because of the presence of surface, interface, and different sources of inhomogeneities, these nanostructures often undergo internal stresses associated with elastic strains. Due to the size reduction and the fabrication process that are generally conducted far from equilibrium, very high stresses can be localized in small volumes. Stresses of a few GPa and strain of a few percentages are thus commonly reached.

Transmission electron microscopy (TEM) is a powerful tool for structural analysis at the nanometric scale. Its originality is to combine analysis in both direct and reciprocal space. Imaging mode allows localization at the nanoscale and also gives direct and very local information on interfacial morphology and extended defects, while precise measurement of the lattice parameters is achievable through electron diffraction.

This chapter will present how the structural information accessible by TEM can be transformed into stress or strain quantities. Actually this supposes to consider the strain as a variation of lattice parameters. It will be shown that one has to build mechanical models to obtain the full strain or stress tensor from these experimental data. The hypotheses made in this frame and the limits of validity of these hypotheses will be discussed.

After some brief recalls on elasticity and on TEM principles, we will introduce in Section 9.1 one of the main issues encountered in TEM analysis, the thin foil relaxation effect. Sections 9.2 and 9.3 will be devoted to two methods where the thin foil relaxation can be efficiently exploited as a probe of stress or strain, the TEM curvature and the convergent beam electron diffraction (CBED); in both of these methods, the sample thicknesses, in the range of 100–500 nm, can be measured accurately. Section 9.4 will discuss some issues specific to strain determination from high-resolution electron microscopy (HREM) image analysis, which can be applied to very thin samples.

Mechanical Stress on the Nanoscale: Simulation, Material Systems and Characterization Techniques, First Edition.
Edited by Margrit Hanbücken, Pierre Müller, and Ralf B. Wehrspohn.
© 2011 Wiley-VCH Verlag GmbH & Co. KGaA. Published 2011 by Wiley-VCH Verlag GmbH & Co. KGaA.

9.1 Introduction: How to Get Quantitative Information on Strain from TEM

9.1.1 Displacement, Strain, and Stress in Elasticity Theory

In a continuous description of the matter, the strain ε is a tensor of rank 2 expressing the derivative of a displacement field U with respect to a reference state. In the first-order approximation, the strain components in a given basis are

$$\varepsilon_{ij} = \frac{1}{2}\left(\frac{\partial U_i}{\partial x_j} + \frac{\partial U_j}{\partial x_i}\right) \tag{9.1}$$

where U_i and U_j are the components of U in this basis. Internal forces can be represented by the means of a tensor of rank 2, the stress tensor σ, which has the dimension of a force per area unit (N/m^2 or Pa). In the frame of the linear elasticity, the strain and stress are linearly linked by the elasticity (or stiffness) tensor C (Hooke's law):

$$\sigma = C\varepsilon \tag{9.2}$$

In crystals, which are anisotropic by nature, C is a tensor of rank 4 containing 3–21 independent elastic coefficients, depending on the crystal symmetry.

It ensues from these definitions several important consequences on strain measurements:

- Any passage from strain to stress (and conversely) supposes that the elastic coefficients of the material are known.
- Determining the strain state of a material supposes to define a "reference state" or "relaxed state," the one that the material would adopt without internal or external stresses. This relaxed state is often assimilated to the bulk state, which can be problematic in case of a metastable material that does not exist in the bulk state.
- The continuous concepts defined here are valid only at a scale larger than the lattice spacing. When the nanocrystal is formed by a few atomic planes, the lattice distortions are better described by atomic models.

9.1.2 Principles of TEM and Application to Strained Nanosystems

Crystalline materials can be explored in both diffraction and image modes (Figure 9.1). Due to the objective lens, the electron beams that have gone through the sample can be focused. If the incident beam is parallel, the diffracted and transmitted beams can be focused in the focal plane of the objective lens. By using a suitable intermediate lens, the diffraction pattern formed in the focal plane can be projected onto the screen (diffraction mode). The main modes of image formation are schematically represented in Figure 9.1b:

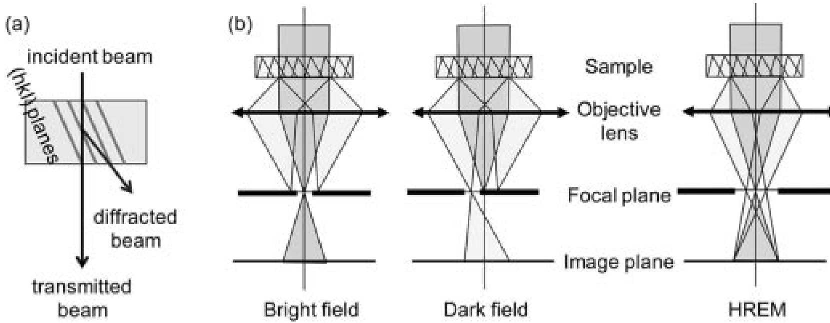

Figure 9.1 Principles of TEM. (a) Diffraction by a crystal. (b) Principle of the image formation from the transmitted beam (bright field), from a single diffracted beam (dark field), or from interference of several beams (HREM mode).

- **Conventional imaging:** The image is formed here either by the transmitted beam (bright field) or by one of the diffracted beams (dark field). The chosen beam is selected by an aperture located in the focal plane. The contrast in the image is due to variations of diffraction conditions in the sample.
- **HREM imaging:** The contrast here results from the interference of several beams, diffracted and transmitted, that produces a phase contrast. If an (*hkl*) family of planes parallel to the beam has an interplanar distance d_{hkl} larger than the point resolution of the microscope (typically 0.1–0.2 nm), the image present parallel lattice fringes with a spacing corresponding to d_{hkl}. Most often, the electron beam is chosen parallel to a crystallographic direction with a high symmetry, called zone axis. If more than one family of lattice fringes are observed, the image looks like a 2D projection in this direction of the atomic columns of the 3D crystal.

The strain, as defined by the elasticity theory in Section 9.1.1, is never directly measured in a TEM experiment. In fact, to get information on strain, one assimilates strain components to variations of lattice parameters that can be deduced either from a direct analysis of electron diffraction patterns or from analysis of high-resolution images.

9.1.3
A Major Issue for Strained Nanostructure Analysis: The Thin Foil Effect

Transparency to electrons depends on the electron wavelength and on the extinction distance, specific to the material and the diffracting planes. Conventional imaging (dark and bright fields) and diffraction are possible up to a few hundreds of nanometers. HREM imaging requires even smaller thickness, below 50 nm. Various techniques of thinning, including mechanical polishing, chemical etching, ion milling, and focused ion beam, are used to achieve the electron transparency. Alterations like surface amorphization or partial annealing are possible, but are likely to be limited by a careful use of these thinning methods.

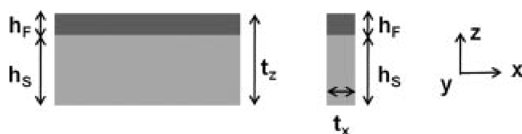

Figure 9.2 Sample geometry: the direction of observation is *z* in plane view (left) and *x* in cross section (right).

More annoying for the purpose discussed here is the creation of free surfaces with a major consequence: a change in the strain state. Stress relaxation in periodic superlattices has been the object of a theoretical work in 1985 by Treacy and Gibson [1, 2]. The considered system was a [001]-oriented strained superlattice in a cubic material. Using Fourier series, the authors have analytically calculated the strain gradient generated by the cross-sectional thinning along one [100] direction of the interface plane. The main conclusions of this early study can be qualitatively generalized to a single layer: the level of relaxation is fixed by the ratio between the thickness of the foil along the thinned direction, t_x, and the thickness of the strained layer, h_F (Figure 9.2). Schematically, if t_x is much larger than h_F, the stress remains biaxial; as t_x decreases, the symmetry of stress and strain tensors is reduced and one tends to a full relaxation of the stress along the direction of observation and uniaxial stress along the perpendicular direction [1, 2].

Inhomogeneous strain fields and a reduction of the average strain in agreement with the theoretical model [1, 2] have been experimentally observed in InAlAs superlattices [3]. Single layers also exhibit experimental values of strain smaller than that expected [4, 5]. Finite element modeling (FEM) is now used to calculate numerically surface relaxation effect when analytical models are not suitable [6, 7].

In the following sections, we will review the main manifestations of the strain relaxation and some possible strategies to achieve the initial strain state from a thinned sample.

9.2 Bending Effects in Nanometric Strained Layers: A Tool for Probing Stress

9.2.1 Bending: A Relaxation Mechanism

Bending is a well-known mechanism of relaxation that occurs in any bilayer system with a finite size, independent of the origin of stress (Figure 9.3a). The TEM samples do not escape this phenomenon. Figure 9.3b is a scanning electron microcopy (SEM) observation of a 10 nm $Ga_{0.8}In_{0.2}As$ layer epitaxially grown on a GaAs substrate, after it has been thinned from the substrate side for plane-view TEM observation. The foil is characterized by a strong bending of the thinned zones. Cleavage also occurred spontaneously during the thinning. In this example, bending is a clear manifestation of the relaxation of the epitaxial stress in the layer that is due to elastic accommodation

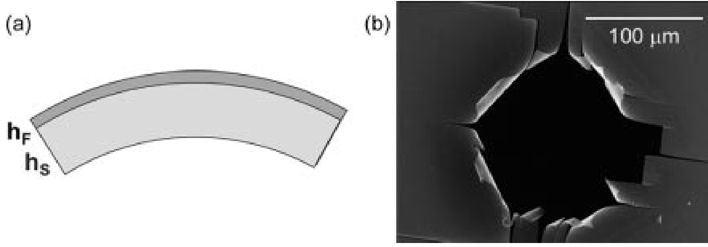

Figure 9.3 Curvature of a bilayer system with a finite size. (a) Schematic representation in section. (b) SEM observation of a 10 nm $Ga_{0.8}In_{0.2}As$ layer epitaxially grown on a (001) GaAs substrate after thinning by the substrate side for plane-view TEM observation.

of lattice mismatch with the substrate. This can be generalized to internal stresses of any origin.

Using bending of TEM specimen as a probe of stress appears highly attractive; it requires

- a reliable relation between the internal stress and the curvature, and
- a means of measurement adapted to TEM specimens.

9.2.2 Relation between Curvature and Internal Stress

Let us first consider the stress in the layer for an infinite substrate. The stress tensor can be expressed in a (x, y, z) orthogonal basis, where z is the direction normal to the surface (Figure 9.2). From mechanical considerations, it comes that each component of stress along z is null (the surface being free):

$$\sigma = \begin{pmatrix} \sigma_{xx} & \sigma_{xy} & \sigma_{xz} \\ \sigma_{xy} & \sigma_{yy} & \sigma_{yz} \\ \sigma_{xz} & \sigma_{yz} & \sigma_{zz} \end{pmatrix} = \begin{pmatrix} \sigma_{xx} & \sigma_{xy} & 0 \\ \sigma_{xy} & \sigma_{yy} & 0 \\ 0 & 0 & 0 \end{pmatrix} \tag{9.3}$$

In addition, if the stress is isotropic in the (x, y) plane, the stress tensor is entirely characterized by a single term, the in-plane component σ_0:

$$\sigma = \begin{pmatrix} \sigma_0 & 0 & 0 \\ 0 & \sigma_0 & 0 \\ 0 & 0 & 0 \end{pmatrix} \tag{9.4}$$

In crystalline layers, this situation can occur if z is a direction of high-crystalline symmetry and the stress in the (x, y) plane is biaxial. For a finite size of the substrate (Figure 9.3a), the analytical model of Timoshenko [8, 9], based on the equilibrium of the forces and of the moments, establishes a linear relation between the curvature κ and the "initial" stress σ_0:

$$\frac{1}{\kappa} = R = \frac{E_S h_S^2}{6(1-\nu_S)h_F\sigma_0} F(\delta,\eta),$$
$$\text{where } F(\delta,\eta) = \frac{1+4\eta\delta+6\eta\delta^2+4\eta\delta^3+\eta^2\delta^4}{1+\delta}, \quad \eta = \frac{E_F(1-\nu_S)}{E_S(1-\nu_F)}, \text{ and } \delta = \frac{h_F}{h_S} \tag{9.5}$$

Here R is the radius of curvature, E_S is the Young's modulus, ν_S is the Poisson's ratio, and h_S is the thickness of the substrate; E_F is the Young's modulus, ν_F is the Poisson's ratio, and h_F is the thickness of the thin film. The function $F(\delta, \eta)$ reflects the transfer of the stress from the layer toward the substrate associated with the specimen bending [8, 9]. When the layer thickness h_F is negligible with respect to the substrate thickness h_S, that is, when $F(\delta, \eta)$ tends to 1, Eq. (9.5) is known as the Stoney's formula [10]. This calculation can be generalized for multilayered structures [11].

Determining the stress, in a layer from the substrate bending is a well-known procedure; X-ray diffraction or optical reflectometry are well-suitable techniques for measuring radius of curvature in the range of 1–100 m and are generally applied to substrates whose thickness is some hundreds of micrometers [12, 13].

Examination of Eq. (9.5) indicates a huge exaltation of the bending effect due to thinning in plane-view TEM specimens. For instance, a radius of 1 m for a 100 μm thick substrate becomes 1 μm after thinning to 100 nm.

9.2.3
Using the Bending as a Probe of the Epitaxial Stress: The TEM Curvature Method

Conventional TEM provides reliable and accurate methods to measure the curvature in the range of 10–200 μm and the foil thickness in the range of 100–500 nm [14]. In bright field (Figure 9.1b), there is a deficit of the amplitude of the transmitted beam in the places where an (*hkl*) family of crystal planes is in Bragg position. Due to the foil curvature, these regions are in symmetrical positions with respect to the incident beam (Figure 9.4a) and dark lines called bend contours appear in the image (Figure 9.4b). Applying the Bragg law, the radius of curvature R is very directly linked to the distance D_0 between the bend contours, following

$$R = D_0/2\sin\theta = D_0 d_{hkl}/\lambda \tag{9.6}$$

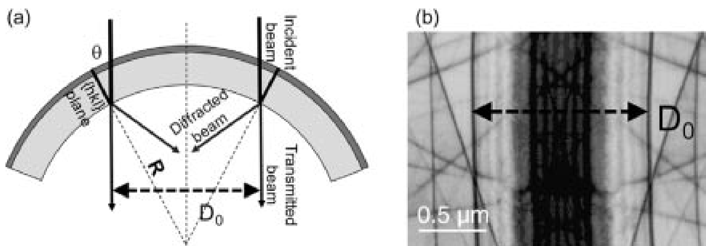

Figure 9.4 Bend contours in a curved bilayers. (a) Formation of the bend contours. (b) Bright field image in plane-view; the diffracting planes are (220) (same sample as in Figure 9.3b).

where θ is the Bragg angle, d_{hkl} is the interplanar distance of the diffracting planes (*hkl*), and λ is the electron wavelength [14]. A precision of about 2% on R is achieved.

The foil thickness t_z (Figure 9.2) can be measured from diffraction contours in dark field with a method derived from that used for CBED [15] and adapted to take into account the curvature [14]. This measure is very precise (better than 2%) for thicknesses in the range of a few hundreds of nanometers.

An example of stress determination in a nanometric layer using the curvature is given in Figure 9.5. The thinning process has produced a slow variation of h_s, which allows to fit the Timoshenko's relation over the range of 100–300 nm. The unique adjustable parameter is the in-plane component of the stress σ_0 [14].

9.2.4 Occurrence of Large Displacements in TEM Thinned Samples

The analytical approach described above uses the simplified theory of elasticity with the hypothesis of small displacements. A simple criterion for small displacements is that the deflection, that is, the total displacement perpendicularly to the sample, is small compared to the radius of curvature. Break of the linearity between stress and curvature is predicted in case of large deflections [9] and has been observed in micrometric samples [16]. It turns out that TEM foils are much more bent than in the classical curvature method.

It is thus legitimate to question the validity of the Timoshenko's approach [17]. The occurrence of large displacements is related to the lateral extension of the

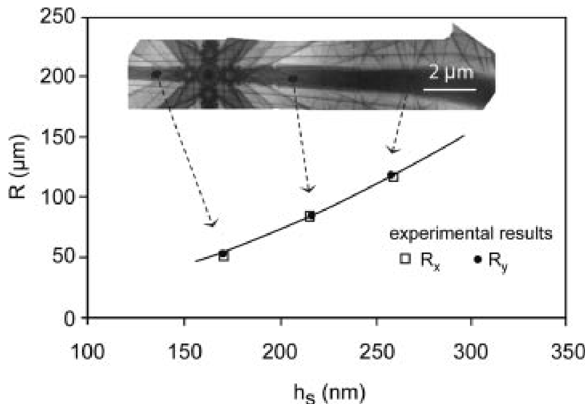

Figure 9.5 Stress determination in a 10 nm thick $Ga_{0.8}In_{0.2}As$ layer on a GaAs substrate. *Inset*: The cleavage occurred during the plane-view thinning has resulted in a rectangular lamella (here in bright field). *Curve*: Radius of curvature R_x and R_y, measured in bright field in two directions, reported as function of the substrate thickness h_s, measured in dark field. One obtains σ_0, the in-plane component of epitaxial stress before thinning, by fitting the experimental points with Eq. (9.5) (full line). Here $\sigma_0 = -1.30 \pm 0.16$ GPa.

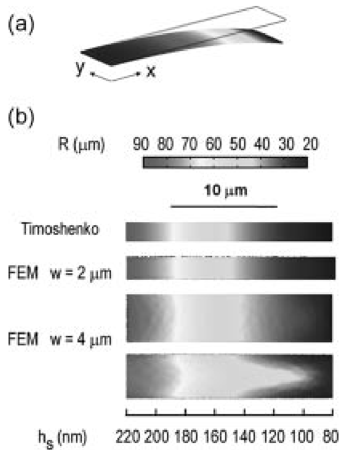

Figure 9.6 (a) FEM of a 10 nm GaInAs layer on a GaAs substrate. The substrate thickness h_s varies linearly from 80 to 220 nm. (b) Projection in the (x–y) plane of the radius of curvature R. *Top to bottom*: Analytical calculation (Timoshenko's formula); FEM when the lamella width is 2 μm; FEM when the lamella width is 4 μm (R is shown in the two main directions).

sample [9], which is not considered in Eq. (9.5). An answer can be given case-by-case using a numerical method like the finite element method. So, for a rectangular lamella with a width W, the curvature presents different regimes as the dimensionless parameter $W^2/(Rh_s)$ increases [17] (independent of the intrinsic characteristics of the strained layer):

- **Small displacements:** The Timoshenko's relation is applicable and the curvature is isotropic (Figure 9.6).
- **Intermediate situation (when $W^2/(Rh_s)$ increases):** A reduction of curvature compared to the Timoshenko's relation and a dissymmetry of the two main curvatures appear (Figure 9.6).
- **Very large displacements:** The curvature becomes cylindrical (Figure 9.7).

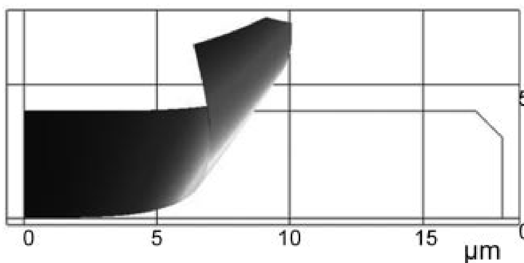

Figure 9.7 FEM of an ultrathin lamella ($h_s = 50$ nm). A full cylindrical curvature is achieved. Cylindrical rollers comparable to this modeling can be observed experimentally in Figure 9.3b.

9.2.5 Advantages and Limits of Bending as a Probe of Stress in TEM

The TEM curvature method appears as particularly suitable to measure stresses on the order of magnitude of a few GPa in epitaxial layers [14, 18]. The principle of this method makes it a very reliable approach from the mechanical points of view [17]:

- The mechanical behavior of the thinned sample is completely controlled.
- The thin foil relaxation effect is not seen as a problem, rather it is the basis of the stress determination principle.
- One measures an element of stress tensor (or the force exerted by the layer on the substrate), while CBED and HREM (being sensitive to atomic positions) measure elements of strain tensor.
- The complete determination of the stress tensor is achieved from this single element, provided that the stress is uniform and biaxial in the film plane.
- The TEM curvature method does not need a reference zone in the substrate.
- The knowledge of the relaxed state of the strained layer is not necessary.

Due to the problematic of large displacements, attention should nevertheless be paid to the theoretical frame used to link the curvature with the stress. FEM is an essential tool to determine in which limits the analytical models can be applied [17].

The main drawback is the spatial resolution in the layer plane, on the order of magnitude of the distance between the contours of extinction (typically 1 μm) [14].

9.3 Strain Analysis and Surface Relaxation in Electron Diffraction

9.3.1 CBED: Principle and Application to Determination of Lattice Parameters

Using a convergent beam for electron diffraction experiments (CBED) instead of a parallel beam offers the combined advantages of very small probes and remarkable sensitivity to small variations of the lattice parameters (down to 10^{-4}). Such properties are due to the basic principle of CBED:

- The incident electron beam forms a cone converging onto the sample with a probe size as small as 1 nm.
- The sample is probed at the same time by beams having different incident angles so that many lattice planes families are simultaneously in Bragg position.

All the beams having the same angle of incidence with a given lattice plane belong to a same plane. When the incident angle is a Bragg angle for the lattice plane, all these beams are diffracted and intercept the focal plane along a line (excess line) (Figure 9.8a). As a consequence, a deficiency line parallel to the excess line is formed in the transmitted beam. In fact, due to the conical shape of the beam, the CBED

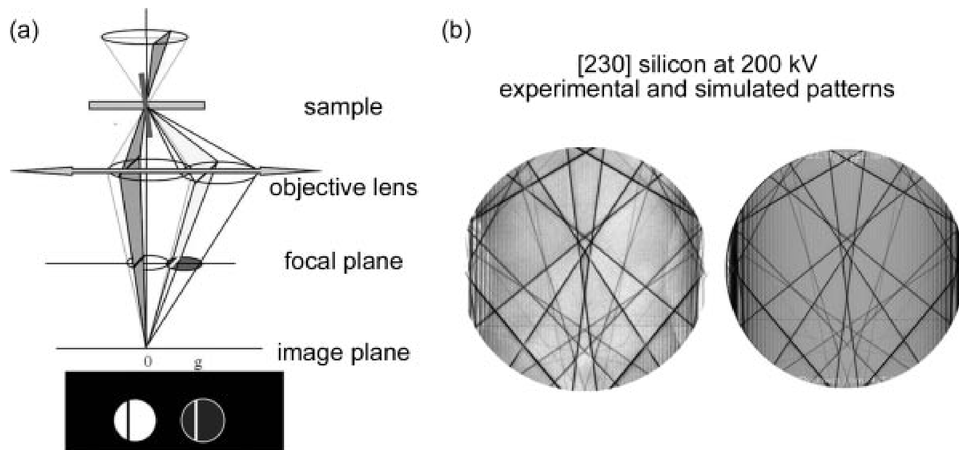

Figure 9.8 Principle of CBED. (a) Diffraction in convergent beam. (b) Experimental diagram (filtered) at 200 kV, in a [230]-oriented silicon crystal, and simulated pattern simulated with JEMS software.

pattern is formed by disks instead of spots. The transmitted (or central) disk thus shows numerous dark lines (deficiency lines), each of them corresponding to a particular lattice plane family (Figure 9.8a). All these lines make precise angle between them and their intersection highly depends on the six unit cell parameters (a, b, c, α, β, γ).

Without going further into the details of the technique, let us just mention that a large part of the information included in a CBED pattern comes from the high-order Laue zones (HOLZ) of the reciprocal lattice, which means that the pattern contains 3D information. Thus, most of the deficiency lines displayed in the central disk (all the thin ones) are in fact HOLZ lines.

CBED is highly valuable for investigating the structure in a given area of a specimen: this goes from local variation of the lattice parameters to complete determination of the space group. The lattice parameters are determined through the comparison with simulated patterns (Figure 9.8b). The adjustable parameters required for the simulation are as the following:

- The energy of the electron beam (or microscope voltage) that can be accurately measured from a CBED pattern taken in an unstrained region of a reference crystal.
- The specimen thickness that can be precisely determined from the analysis of the fringes displayed in ZOLZ lines (zero-order Laue zone) of the CBED pattern [15].
- The six unit cell parameters.

Note that suitable patterns require thickness in the range of 200–500 nm. Besides, energy filtering of the recorded pattern in order to suppress inelastic contributions gives enhanced precision. An example is displayed in Figure 9.8b, which shows an experimental pattern together with a simulated one.

9.3.2 Strain Determination in CBED

CBED patterns can be analyzed in terms of elastic strain by comparing the six lattice parameters introduced in the model to fit the experimental pattern with the ones of the relaxed material. The sensitivity can be as good as 10^{-4}. In addition, the local variation of the lattice parameters in different regions of a specimen can be recorded with a high spatial resolution of a few nanometers. Such analyses have been successfully carried out in cross-sectional [19–21] as well as in plane-view specimens [22].

A more complicated situation arises when we try to investigate nano-objects and, in particular, strained epilayer with nanometer thickness. In such cases, only cross-sectional investigations are likely to produce suitable patterns. However, it comes out that the CBED pattern in the epilayer is completely blurred [20]. More precisely, the CBED pattern evolves from a "classical" pattern [23], observed in the substrate at a distance far from the layer/substrate interface, to more complex patterns in which the HOLZ lines progressively change from single to multiple lines with complex profiles (Figure 9.9a). The HOLZ lines thus widen in bands, while the probe approaches the interface, until the pattern is fully blurred.

To understand what happens in this case, it is useful to model the whole specimen (epilayer and substrate) with suitable thickness. Such model is displayed

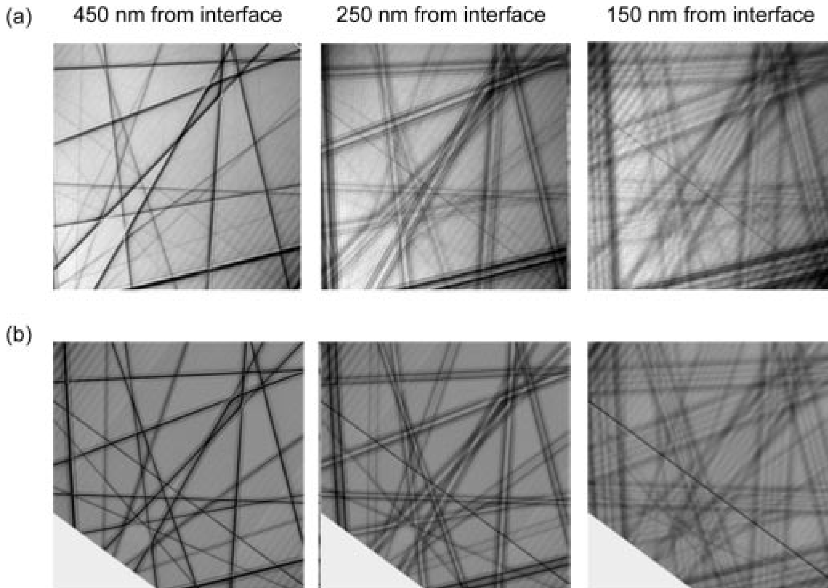

Figure 9.9 [230] CBED central disks of a cross-sectional $Si_{0.8}Ge_{0.2}/Si$ specimen; the foil thickness is 300 nm. (a) Experimental patterns taken in the substrate at respectively 450, 250, and 150 nm from the interface with the epilayer. (b) TDDT simulated patterns taking into account the inhomogeneous strain field calculated by FEM [23, 26].

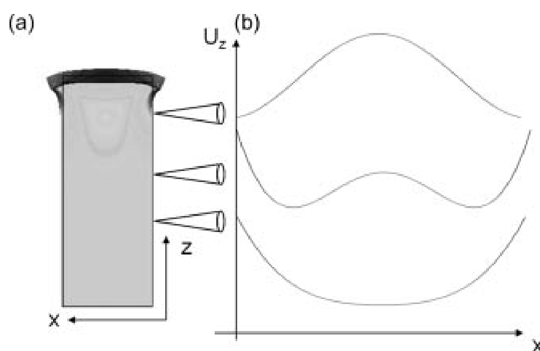

Figure 9.10 FEM of the inhomogeneous strain field in a cross-sectional $Si_{0.8}Ge_{0.2}/Si$ specimen. (a) Map of the U_z displacements. (b) Shape of the U_z profile in the substrate at different distances from the interface.

in Figure 9.10, after free surface relaxation has been calculated through finite element modeling. Clearly, the thin foil effect results in both slight bending of the specimen free surfaces and inhomogeneous strain states in the substrate, until depth is as high as 300 nm from the interface.

As the convergent beam probes the 3D reciprocal lattice, it encounters regions with different states of strain while crossing the specimen thickness at a position close to the interface. It has been shown that the complex line profiles (also called HOLZ line splitting) come from such strain inhomogeneities [24]. Fortunately, several authors [23, 25–27] have developed new approaches to simulate the interaction of the convergent beam with this kind of specimens. Such methods hence provide accurate determination of the initial state of strain in the epilayer from the analysis of the substrate at different positions below the interface, as shown in Figure 9.9b in which the simulations were performed using our home-made software [26] based on the time-dependent dynamical theory (TDDT) approach [28].

In plane view, CBED patterns obtained from an epilayer on a substrate are also affected by the inhomogeneous strain due to the bending described in Section 9.2; in such case, the thinning method has been found to influence the degree of bending [29], making the comparison with simulated patterns even more complex.

9.3.3
Use and Limitations of CBED in Strain Determination

In principle, CBED allows to explore the lattice parameters in the three directions from a single diffraction pattern. When the CBED pattern is not blurred by surface relaxation effects, a direct determination of the strain is possible with a sensitivity of 10^{-4} and a localization at the scale of a few nanometers.

In the more complex situation of heavily strained regions undergoing surface relaxation effects, quantitative modeling of CBED patterns can nevertheless be performed. This requires a complete model, including the initial strain field, a good knowledge of the thinned sample geometry, the displacement field in the thinned

sample, and a good knowledge of the electron probe position on the sample. Application of this principle to strained epilayers has allowed using surface relaxation in the substrate as a probe of the initial strain undergone by the epilayer, with a precision of about 10%.

CBED contains some other limitations and drawbacks: it requires defect-free specimens. This is not so obvious at the scale of TEM investigations. For instance, semiconductors and eventually oxides are much better specimens for CBED than metals that contain many defects due to lower fault energies. Even more important, CBED does not avoid the need for a reference state, as described in Section 9.1.1.

9.3.4
Nanobeam Electron Diffraction

In principle, lattice parameters can be determined simply from the position of the spots in electron diffraction diagrams performed with a parallel beam. However, the large illumination of the sample in the diffraction mode inhibits its use for local strain determination. Nowadays the nanobeam electron diffraction (NBED) mode allows to achieve beams almost parallel to a probe as small as a few nanometers. Strain variation of about 10^{-3} can be detected at the scale of 10 nm [30]. Recently a resolution of about 2.7 nm and a sensitivity of 6.10^{-4} have been reported [31]. As CBED, NBED necessitates a comparison of experimental and simulated strain profiles to take into account the thin foil relaxation phenomena [31] and it does not escape the use of a reference state.

9.4
Strain Analysis from HREM Image Analysis: Problematic of Very Thin Foils

9.4.1
Principle

An HREM image can be considered as a sum of individual lattice fringes, each set of fringes displaying its own spatial frequency g. Strain determination consists in measuring precisely the lattice fringes spacing in an HREM image and determining a 2D displacement field u compared to a reference area in the image, displaying lattice fringes of well-known spacing (Figure 9.11). Two techniques are used:

- The position of each "atomic column" can be determined directly *in the image* using a peak finding procedure [32, 33].
- The variation in the fringe spacing from one region to another can also be measured *in the Fourier space*, through Fourier filtering around the spatial frequency g of interest (geometrical phase analysis (GPA)) [34]. The inverse Fourier transform after Fourier filtering produces a complex image, whose phase

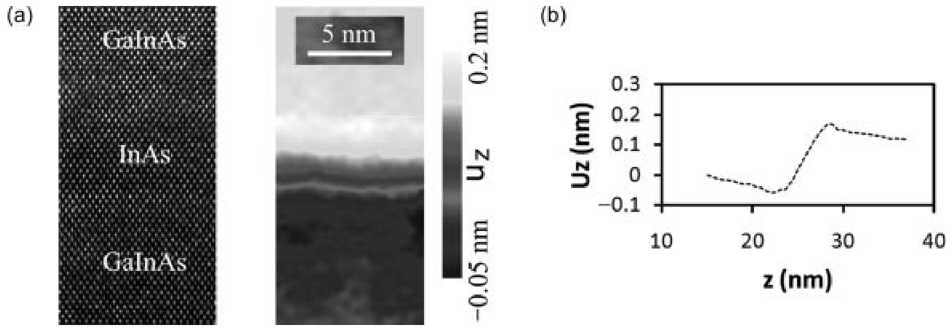

Figure 9.11 HREM analysis of a strained InAs quantum well inserted between two $Ga_{0.47}In_{0.53}As$ barriers with a nominal lattice mismatch of 0.032 [5]. (a) ⟨110⟩ zone axis image and map of u_z, the displacements in the growth direction z (GPA method). (b) Profile of u_z in the growth direction z.

P_g displays the local variation Δg of the spatial frequency (phase shift) in each point of the image. The local displacement u of the fringes is directly related to the phase shift.

$$P_g = -2\pi g \cdot u \tag{9.7}$$

When two different sets of fringes are selected, each having its own spatial frequency g_1 and g_2, two components of displacement (u_1, u_2) can be determined. It is thus obtained a 2D displacement field U^{2D}, whose derivative with respect to the spatial positions x_i, x_j (in an orthogonal basis) defines a 2D "strain" tensor ε^{2D}:

$$\varepsilon_{ij}^{2D} = \frac{1}{2}\left(\frac{\partial U_i^{2D}}{\partial x_j} + \frac{\partial U_j^{2D}}{\partial x_i}\right) \tag{9.8}$$

Strain determination thus consists in assimilating this 2D "strain" field, measured from the image, to the 2D projection of the strain tensor ε occurring in the crystal, as defined in Section 9.1.1 (or assimilating the 2D displacement field U^{2D}, measured from the image, to the 2D projection of the 3D displacement field U occurring in the crystal).

The smallest displacement that can be measured is around 1 pm in optimal conditions [35] (in practice, it can be larger due to different sources of noise). The spatial resolution is not limited by the point resolution of the microscope (that determines which lattice fringes can be analyzed), but rather due to the image analysis principle. For peak finding procedures, averaging over neighboring columns can be necessary to improve the signal-to-noise ratio, which impacts the spatial resolution. For GPA, the spatial resolution is intrinsically limited by the use of a mask selecting the g frequency in the Fourier space of the image [34]. Using the largest filter, the resolution cannot be better than two times the distance between the analyzed fringes (in a semiconductor, this corresponds to about 0.6 nm when (002) planes are analyzed).

9.4.2
What Do We Really Measure in an HREM Image?

The very good resolution made HREM highly attractive for strain determination in nano-objects. Nevertheless, despite its apparent simplicity, this is not a straightforward method. Actually, issues of different nature are hidden in the approach consisting in assimilating the 2D strain field ε^{2D} determined in the image to the 2D projection of the actual 3D strain field.

9.4.2.1 **Image Formation**

Independent of the strain issue, considering the lattice fringes as the 2D projection of the atomic planes throughout the whole crystal is an approximation. In fact, two main sources of artifacts are possible when analyzing image contrasts:

- **Inhomogeneities in the specimen:** Due to the nature of the contrast in HREM, any change in the beam phase, as those due to thickness gradients or bending in the thinned sample, shifts the position of the lattice fringes in the image.
- **Transfer function of the objective lens:** Spherical aberration of the lens is specifically responsible for delocalization effects near interfaces (the lattice fringes in the images are shifted with respect to the exact projection of the lattice planes in the crystal).

These points can be fully or partially controlled by a careful preparation of the thinned sample, the use of new generation of TEM as those equipped with a corrector of spherical aberration, and the help of image simulation [6, 7].

9.4.2.2 **Reconstruction of the 3D Strain Field from a 2D Projection**

Let us express the strain tensor by the following matrix in a (x, y, z) orthogonal basis, where x is the direction of observation (Figure 9.2):

$$\varepsilon = \begin{pmatrix} \varepsilon_{xx} & \varepsilon_{xy} & \varepsilon_{xz} \\ \varepsilon_{xy} & \varepsilon_{yy} & \varepsilon_{yz} \\ \varepsilon_{xz} & \varepsilon_{yz} & \varepsilon_{zz} \end{pmatrix} \quad (9.9)$$

The components ε_{yy}, ε_{zz}, and ε_{yz} are, in principle, related to the components of the strain tensor ε^{2D} determined from the HREM image, as described in Section 9.3.1 (Eq. (9.8)), but the other components (along the direction of observation) are missing data. To reconstruct the full strain tensor, several steps are generally necessary. To illustrate this reconstruction step-by-step, let us consider the simple and usual situation displayed in Figure 9.11 of a [001]-oriented layer in a cubic system, grown on a cubic substrate with a lattice mismatch f. We suppose that the in-plane symmetry is preserved by the epitaxial growth (for a more general approach including any orientations, see Ref. [36]). y is the in-plane direction perpendicular to x and z is the growth direction.

- **Removing the reference for zero strain:** Measurements in the image are carried out by comparing the lattice fringes spacing in the area of interest with their

spacing in a reference area supposed unstrained. In practice, this reference is not always the studied material in its relaxed state, but it is most often another material. To deduce the strain tensor ε, one has to first remove a contribution due to this reference. The reference is often the substrate; in such case, its contribution is expressed in terms of the lattice mismatch f between the relaxed material and the substrate:

$$\varepsilon_{yy} = \varepsilon_{yy}^{2D} - f \quad \text{and} \quad \varepsilon_{zz} = \varepsilon_{zz}^{2D} - f \tag{9.10}$$

It is worth noting that f is one of the unknown values that one intends to measure.

- **Elaborating a physical model of deformation:** To go further, one needs a model of deformation including some hypotheses. Here, a simple model is that the layer is fully strained so that the in-plane strains are imposed by the lattice mismatch ($\varepsilon_{xx} = \varepsilon_{yy} = -f$) and the stress is biaxial ($\sigma_{xx} = \sigma_{yy} = \sigma_0$) as in Eq. (9.4).
- **Use of a law of elastic behavior:** A law of elastic behavior, here the Hooke's law (9.2) relating the strain and stress through the elastic coefficients, is also necessary. By application of Eq. (9.2), it comes

$$\varepsilon_{zz} = -2\frac{C_{12}}{C_{11}}\varepsilon_{xx} \quad \text{and} \quad f = \frac{\varepsilon_{zz}^{2D}}{1-2(C_{12}/C_{11})} \tag{9.11}$$

The problem, that is, determining of both the relaxed and strained states of the layer from the image analysis, is now completely solved, on the basis of several hypotheses:

- The experimental reference of "zero" strain is supposed perfect and unstrained.
- Here, a full elastic accommodation of the lattice mismatch has been supposed. Other models, including interfacial dislocations or anisotropic accommodation, are possible.
- The law of elastic behavior necessitates the knowledge of the elastic properties of the strained layer (here the C_{ij}).
- The status of the x-direction in the model is probably the most delicate point, as detailed in the next section.

9.4.3 Modeling the Surface Relaxation in an HREM Experiment

9.4.3.1 Full Relaxation (Uniaxial Stress)

In the model developed above, surface relaxation was ignored. A full relaxation implies $\sigma_{xx} = 0$ and leads to a different solution. In case of a $\langle 110 \rangle$ direction of observation,

$$\begin{aligned} \varepsilon_{xx} &= \frac{C_{11}(C_{11}+C_{12}-2C_{44})-2C_{12}^2}{C_{11}(C_{11}+C_{12}+2C_{44})-2C_{12}^2} f \\ \varepsilon_{yy} &= -f \\ \varepsilon_{zz} &= \frac{4C_{12}C_{44}}{C_{11}(C_{11}+C_{12}+2C_{44})-2C_{12}^2} f \end{aligned} \tag{9.12}$$

With typical values of C_{ij} in semiconductors, the ε_{zz} component and the measured strain ε_{zz}^{2D} are now reduced by about 50% and 30%, respectively, compared to the biaxial case.

9.4.3.2 Intermediate Situations: Usefulness of Finite Element Modeling

Intermediate situations can be evaluated either analytically in some cases as proposed by Treacy and Gibson [1, 2] or numerically using atomistic modeling or FEM [5–7]. Figure 9.12a displays, for instance, displacement profiles across a 5 nm InAs strained layer embedded in two GaInAs buffers lattice matched to InP. The nominal lattice mismatch is 0.032. The profiles are calculated by FEM for two foil thickness t_x (45 and 13 nm) and compared with the nominal displacement without relaxation [5]. The two main features are as the following:

- The transfer of stress from the layer to the buffers, which is attested by the occurrence of negative displacements within the buffers.
- The decrease of the strain within the layer.

This decrease reaches 10% when the foil thickness is 20 times the layer thickness (Figure 9.12b). This indicates that the situations where the relaxation can be neglected are very limited. The reduction of 50% for a full relaxation is in agreement with the analytical approach above.

9.4.3.3 Thin Foil Effect: A Source of Incertitude in HREM

This approach encounters nevertheless some limits:

- While the methods based on extinction contours are very efficient and precise to determine "large" thicknesses (in the range of 100–500 nm for semiconductors),

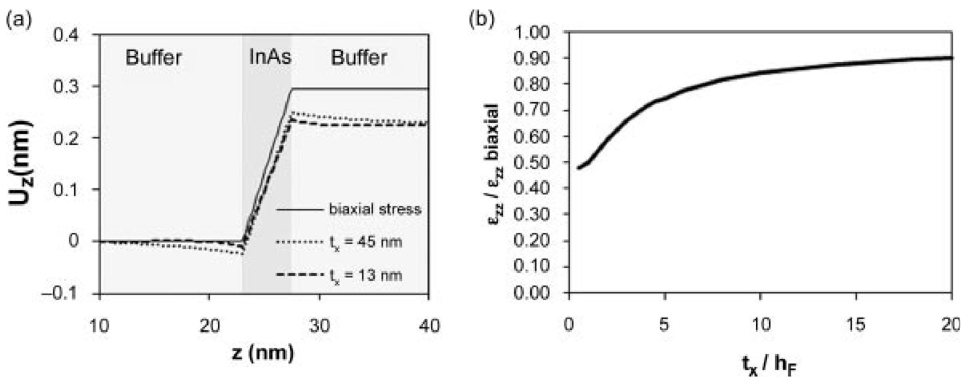

Figure 9.12 FEM of surface relaxation in a 5 nm InAs layer embedded in two $Ga_{0.47}In_{0.53}As$ buffers [5]. The nominal lattice mismatch is 0.032. (a) Out-of-plane displacements for two foil thicknesses t_x (45 and 13 nm) compared with the theoretical profile without relaxation. (b) Normalized out-of-plane strain within the layer as a function of the ratio foil thickness (t_x) over layer thickness (h_F).

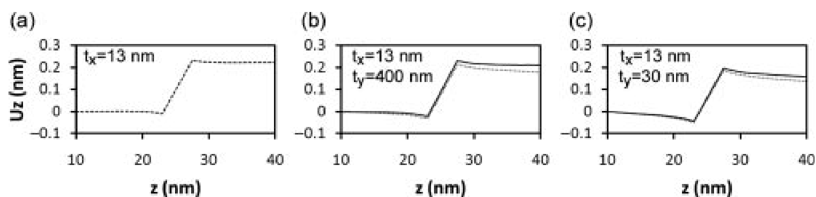

Figure 9.13 Out-of-plane displacements (same sample as in Figure 9.12) modeled with various boundary conditions allowing thin foil effect in one, two, or three directions [5]. (a) Perfect relaxation, only in the *x*-direction (the sample has a finite size t_x of 13 nm along *x* and is infinite along *y*). (b) Additional relaxation is allowed, thanks to a free surface in the *y*-direction, at a distance t_y of 400 nm. In addition, the out-of-plane displacements at the substrate side are either forbidden (full line) or free (dashed line). (c) Same as (b), with t_y of 30 nm.

they fail below a few tens of nanometers. Unfortunately, this corresponds to the range of thicknesses suitable for HREM. In many cases, the foil thickness can just be estimated, which has serious consequences on the precision of the measured strain.

- Due to the very small thickness, it is difficult to fully control the shape of an HREM foil. The examined zone can be “lacework-like,” cleaved, with an inhomogeneous thickness, and so on. The calculated displacements are sensitive to any of these parameters. Figure 9.13a–c shows, for instance, modifications of the displacements when additional thin foil effects are permitted in addition to the main relaxation along the direction of observation. So, the concept of “perfect relaxation” generally adopted in the modeling should be questionable [5].

9.4.4
Conclusion: HREM is a Powerful but Delicate Method of Strain Analysis

HREM image analysis is until now the most local TEM method available to explore strain at the nanoscale and it presents a good sensitivity to displacements. Use of new generation of TEM, like those with a corrector of spherical aberration, makes it even more attractive.

Nevertheless, it is not a direct method to measure strain. On the contrary, it implies a careful mechanical analysis to transform the experimental data – the relative distortions of lattice fringes in a 2D image – into components of a volume strain tensor. Among the various hypotheses chosen for this purpose, the surface relaxation along the thinning direction is particularly susceptible to degrade the reliability of the absolute measurement. Comparison of experimental and simulated displacements is thus necessary to evaluate the precision of the measured strain. Also note that the boundary conditions adopted in modeling are not necessary representatives of the actual situation. So, the concept of “perfect relaxation” generally adopted in the modeling should be questionable.

9.5 Conclusions

With TEM, we have at our disposal a variety of methods to explore internal strain in nanometric crystalline objects. TEM combines a good sensitivity with a fine spatial resolution. Technical improvements in various fields (lenses, energy filtering, image analysis, etc.) have recently upgraded the performances of quantitative TEM; new promising techniques like nanobeam electron diffraction [31] and dark field holography (HoloDark) [37] are in development to explore strain with resolution as good as 3–4 nm.

TEM is nevertheless not a direct method for strain measurement. For this objective, the ability of TEM to explore crystalline materials is exploited: the physical quantities that are experimentally determined are essentially related to lattice parameter variations. To go from these experimental data to the more abstract concept of strain, one has to build mechanical models. They include some or all of the following components:

1) A law of elastic behavior relating strain and stress in the material under study, including a relaxed state of the material.
2) A model of mechanical loading reproducing the physical origin of stress in the sample.
3) A geometrical model of the thinned sample.
4) Boundary conditions.
5) An experimental reference of zero strain.

The validity and the precision of strain or stress assessment depend on the hypothesis made at each step. While the first two components involve physical choices describing the studied system, the others (specimen geometry, boundary conditions, and reference of zero strain) fully depend on the thinning required for TEM experiment.

Indeed, in this approach, one of the most critical points is that TEM measurements are performed on thinned samples, which implies that the strain state has been modified by surface relaxation (thin foil effect). Fortunately, if the sample geometry and boundary conditions are known with precision, the stress or strain before thinning can be calculated with a good reliability, using numerical calculation. Surface relaxation mechanisms can even be used as tools probing the stress before thinning. If the sample geometry and boundary conditions are not known with precision, surface relaxation constitutes one of the main weaknesses of TEM quantitative analysis of strain. In this sense, quantitative analysis of strain methods using relatively thick foils with well-characterized shapes (CBED, TEM curvature, and HoloDark) are more reliable than those using very thin foils (HREM). Nevertheless, HREM remains a highly valuable method, a unique one allowing the strain profile analysis at the scale of the atomic planes.

Keeping in mind these limitations, TEM appears as one of the most powerful techniques for a local investigation of stressed crystalline nanostructures. It offers

various approaches especially well adapted to strained nanometric objects like quantum dots or epitaxial layers.

Acknowledgment

The authors are very pleased to thank N. Combe for critical reading of this chapter.

References

1. Treacy, M.M.J. and Gibson, J.M. (1986) The effects of elastic relaxation on transmission electron-microscopy studies of thinned composition-modulated materials. *J. Vac. Sci. Technol. B*, **4**, 1458–1466.
2. Treacy, M.M.J., Gibson, J.M., and Howie, A. (1985) On elastic relaxation and long wavelength microstructures in spinodally decomposed $In_xGa_{1-x}As_yP_{1-y}$ epitaxial layers. *Philos. Mag. A*, **51**, 389.
3. Seitz, H., Seibt, M., Baumann, F.H., Ahlborn, K., and Schroter, W. (1995) Quantitative strain mapping using high-resolution electron-microscopy. *Phys. Status Solidi A*, **150**, 625–634.
4. Robertson, M.D., Currie, J.E., Corbett, J.M., and Webb, J.B. (1995) Determination of elastic strains in epitaxial layers by HREM. *Ultramicroscopy*, **58**, 175–184.
5. Gatel, C., Tang, H., Crestou, C., Ponchet, A., Bertru, N., Doré, F., and Folliot, H. (2010) Analysis by high-resolution electron microscopy of elastic strain in thick InAs layers embedded in $Ga_{0.47}In_{0.53}As$ buffers on InP(001) substrate. *Acta Mater.*, **58**, 3238.
6. Tillmann, K., Lentzen, M., and Rosenfeld, R. (2000) Impact of column bending in high-resolution transmission electron microscopy on the strain evaluation of GaAs/InAs/GaAs heterostructures. *Ultramicroscopy*, **83**, 111.
7. Rosenauer, A., Gerthsen, D., and Potin, V. (2006) Strain state analysis of InGaN/GaN: sources of error and optimized imaging conditions. *Phys. Status Solidi A*, **203**, 176–184.
8. Timoshenko, S. (1925) Analysis of bi-metal thermostats. *J. Opt. Soc. Am.*, **11**, 233–255.
9. Freund, L.B., Floro, J.A., and Chason, E. (1999) Extensions of the Stoney formula for substrate curvature to configurations with thin substrates or large deformations. *Appl. Phys. Lett.*, **74**, 1987–1989.
10. Stoney, G.G. (1909) The tension of metallic films deposited by electrolysis. *Proc. R. Soc. Lond. A*, **82**, 172–175.
11. Feng, Z.C. and Liu, H.D. (1983) Generalized formula for curvature radius and layer stresses caused by thermal strain in semiconductor multilayer structures. *J. Appl. Phys.*, **54**, 83–85.
12. Chason, E., Yin, J., Tetz, K., Beresford, R., Freund, L.B., Gonzalez, M.U., and Floro, J.A. (2000) *In situ* measurements of stress relaxation during strained layer heteroepitaxy, in *Self-Organized Processes in Semiconductor Alloys*, vol. **583** (eds D. Follstaedt, B. Joyce, A. Mascarenhas, and T. Suzuki), Materials Research Society, pp. 167–175.
13. Sander, D., Enders, A., and Kirschner, J. (1995) A simple technique to measure stress in ultrathin films during growth. *Rev. Sci. Instrum.*, **66**, 4734–4735.
14. Ponchet, A., Cabie, M., and Rocher, A. (2004) TEM measurement of the misfit stress by a curvature method in semiconducting epitaxial system. *Eur. Phys. J.*, **26**, 87.
15. Kelly, P.M., Jostsons, A., Blake, R.G., and Napier, J.G. (1975) Determination of foil thickness by scanning transmission

electron microscopy. *Phys. Status Solidi A*, **31**, 771–780.

16 Finot, M. and Suresh, S. (1996) Small and large deformation of thick and thin-film multi-layers: effect of layer geometry, plasticity and compositional gradients. *J. Mech. Phys. Solids*, **44**, 683–721.

17 Cabie, M., Ponchet, A., Rocher, A., Durand, L., and Altibelli, A. (2005) Geometrical criteria required for the determination of the epitaxial stress from the transmission electron microscopy curvature method. *Appl. Phys. Lett.*, **86**, 191901.

18 Cabie, M., Ponchet, A., Rocher, A., Paillard, V., and Vincent, L. (2004) Transmission electron microscopy and Raman measurements of the misfit stress in a Si tensile strained layer. *Appl. Phys. Lett.*, **84**, 870.

19 Toda, A., Ikarashi, N., and Ono, H. (2000) Local lattice strain measurements in semiconductor devices by using convergent-beam electron diffraction. *J. Cryst. Growth*, **210**, 341–345.

20 Toh, S.L., Li, K., Ang, C.H., Er, E., Redkar, S., Loh, K.P., Boothroyd, C.B., and Chan, L. (2004) High spatial resolution strain measurement of deep sub-micron semiconductor devices using CBED. IPFA 2004: Proceedings of the 11th International Symposium on the Physical & Failure Analysis of Integrated Circuits, pp. 143–146.

21 Senez, V., Armigliato, A., De Wolf, I., Carnevale, G., Balboni, R., Frabboni, S., and Benedetti, A. (2003) Strain determination in silicon microstructures by combined convergent beam electron diffraction, process simulation, and micro-Raman spectroscopy. *J. Appl. Phys.*, **94**, 5574.

22 Cherns, D., Kiely, C.J., and Preston, A.R. (1988) Electron diffraction studies of strain in epitaxial bicrystals and multilayers. *Ultramicroscopy*, **24**, 355.

23 Houdellier, F., Roucau, C., Clement, L., Rouviere, J.L., and Casanove, M.J. (2006) Quantitative analysis of HOLZ line splitting in CBED patterns of epitaxially strained layers. *Ultramicroscopy*, **106**, 951.

24 Chou, C.T., Anderson, S.C., Cockayne, D.J.H., Sikorski, A.Z., and Vaughan, M.R. (1994) Surface relaxation of strained heterostructures revealed by Bragg line splitting in LACBED patterns. *Ultramicroscopy*, **55**, 334.

25 Clement, L., Pantel, R., Kwakman, L.F.T., and Rouviere, J.L. (2004) Strain measurements by convergent-beam electron diffraction: the importance of stress relaxation in lamella preparations. *Appl. Phys. Lett.*, **85**, 651.

26 Houdellier, F., Altibelli, A., Roucau, C., and Casanove, M.J. (2008) New approach for the dynamical simulation of CBED patterns in heavily strained specimens. *Ultramicroscopy*, **108**, 426.

27 Alfonso, C., Alexandre, L., Leroux, C., Jurczak, G., Saikaly, W., Charaï, A., and Thibault-Penisson, J. (2010) HOLZ lines splitting on SiGe/Si relaxed samples: analytical solutions for the kinematical equation. *Ultramicroscopy*, **110**, 285.

28 Gratias, D. and Portier, R. (1983) Time-like perturbation method in high-energy electron diffraction. *Acta Crystallogr. A*, **A39**, 576.

29 Houdellier, F., Jacob, D., Casanove, M.J., and Roucau, C. (2008) Effect of sample bending on diffracted intensities observed in CBED patterns of plan view strained samples. *Ultramicroscopy*, **108**, 295.

30 Usuda, K., Mizuno, T., Tezuka, T., Sugiyama, N., Moriyama, Y., Nakaharai, S., and Takagi, S. (2004) Strain relaxation of strained-Si layers on SiGe-on-insulator (SGOI) structures after mesa isolation. *Appl. Surf. Sci.*, **224**, 113–116.

31 Beche, A., Rouviere, J.L., Clement, L., and Hartmann, J.M. (2009) Improved precision in strain measurement using nanobeam electron diffraction. *Appl. Phys. Lett.*, **95**, 123114.

32 Jouneau, P.H., Tardot, A., Feuillet, G., Mariette, H., and Cibert, J. (1994) Strain mapping of ultrathin epitaxial ZnTe and MnTe layers embedded in CdTe. *J. Appl. Phys.*, **75**, 7310.

33 Bierwolf, R., Hohenstein, M., Phillipp, F., Brandt, O., Crook, G.E., and Ploog, K. (1993) Direct measurement of local lattice distortions in strained layer structures by HREM. *Ultramicroscopy*, **49**, 273.

34 Hytch, M.J., Snoeck, E., and Kilaas, R. (1998) Quantitative measurement of displacement and strain fields from HREM micrographs. *Ultramicroscopy*, **74**, 131.

35 Hytch, M.J., Putaux, J.L., and Penisson, J.M. (2003) Measurement of the displacement field of dislocations to 0.03 Å by electron microscopy. *Nature*, **423**, 270.

36 Yang, K., Anan, T., and Schowalter, L.J. (1994) Strain in pseudomorphic films grown on arbitrarily oriented substrates. *Appl. Phys. Lett.*, **65**, 2789–2791.

37 Hytch, M., Houdellier, F., Hue, F., and Snoeck, E. (2008) Nanoscale holographic interferometry for strain measurements in electronic devices. *Nature*, **453**, 1086–1089.